We are IntechOpen, the world's leading publisher of Open Access books Built by scientists, for scientists

6,900
Open access books available

186,000
International authors and editors

200M
Downloads

Our authors are among the

154
Countries delivered to

TOP 1%
most cited scientists

12.2%
Contributors from top 500 universities

WEB OF SCIENCE™

Selection of our books indexed in the Book Citation Index in Web of Science™ Core Collection (BKCI)

Interested in publishing with us?
Contact book.department@intechopen.com

Numbers displayed above are based on latest data collected.
For more information visit www.intechopen.com

Finite element analysis of wall deflection and ground movements caused by braced excavations

Gordon Tung-Chin Kung
National Cheng Kung University
Taiwan

1. Introduction

Excavation is usually employed in the construction of basement of buildings and underground space of the mass rapid transit and the subway system in urban areas (see Fig. 1). Braced excavation is a complicated soil-structure interaction problem and it is a challenge to engineers to simultaneously ensure the safety of excavation system as well as the integrity of properties adjacent to the excavation site including buildings, structures, and life pipes. In a routine excavation design, engineers usually pay much attention to reaching the safety requirements of excavation design, namely, the stability of excavation system. Many empirical, semi-empirical and numerical methods were developed for evaluating the stability of excavation. The past practical experiences indicated that the accuracy of the existing methods to evaluate the stability of excavation is generally acceptable although the ground conditions at various excavation sites are non-homogeneous and have highly spatial variation. This may be attributed to the employment of a relatively conservative factor of safety in the stability analysis of excavation.

Fig. 1. Photos of constructing the mass rapid transit and subway system in Taiwan

According to the practical experiences, it is found that the damage to buildings adjacent to an excavation was reported occasionally even though the stability of excavation can be

ensured. The economic loss of damage to buildings is considerable and such incidents usually cause the procrastination of construction time limit for the excavation project. As such, the serviceability of structure adjacent to the excavation is usually the key factor and plays the predominant role in the performance-based excavation design.

In practice, any of empirical, semi-empirical, or numerical methods can be adopted to evaluate the serviceability of buildings adjacent to an excavation. For empirical and semi-empirical methods, the procedures for estimating the potential of damage to adjacent buildings generally includes three main elements: 1) prediction of excavation-induced ground movements, 2) evaluation of building deformation caused by excavation-induced ground movements estimated, and 3) evaluation of damage potential of buildings based on the building deformation estimated. In the first element, the estimated free-field ground surface settlement caused by excavation is usually employed to evaluate the building deformation. In practice, the empirical and semi-empirical methods, as shown in Fig.2 and Fig. 3, are often selected to estimate the excavation-induced ground movements.

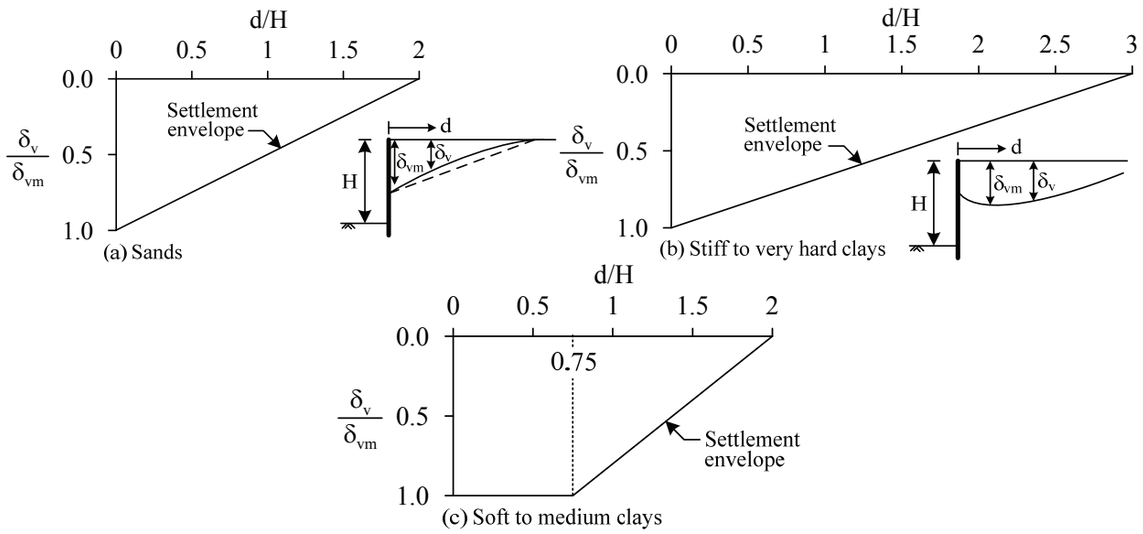

Fig. 2. Design charts for estimating the distribution of surface settlement adjacent to excavation in different soil types (Clough and O'Rourke, 1990)

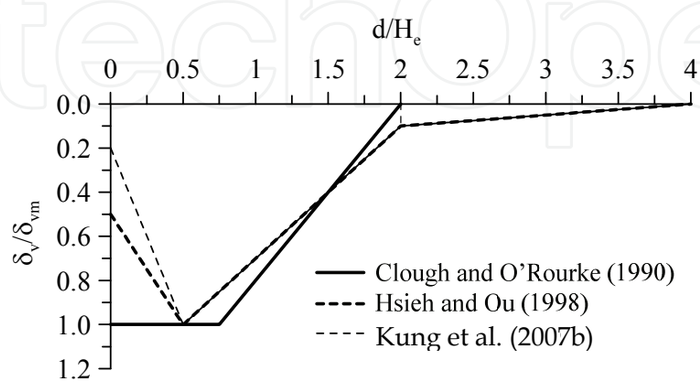

Fig. 3. The ground surface settlement distributions proposed by previous studies for excavations in soft-to-medium clay

It should be noted that these settlement distributions/profiles are established based primarily on the ground surface settlement points monitored in excavation case histories. The applicability of these distributions in the settlement analysis of a new excavation case might be questionable in light of the significant variation of influence factors, such as ground condition and workmanship, between the existing excavation cases and the intended new one. In addition, use of free-field ground surface settlement to estimate the differential settlement of the building may not fully reflect the effect of soil-structure interaction behaviour. It is believed that the ground settlement computed without considering the presence of buildings would be different from that computed with directly incorporating a building into the numerical analysis. Such difference may reduce the accuracy of evaluating damage potential of buildings.

The finite element method (FEM) is often employed to model complex soil–structure interaction problems such as braced excavations. Many investigators (Finno & Harahap, 1991; Hashash & Whittle, 1996; Ng & Yan, 2000; Kung et al., 2007a; Kung et al., 2009) have verified the reliability of FEM applied to analyses of deep excavations even though the uncertainty of soil models and parameters adopted is concerned. Although the deflection of the braced wall can generally be predicted well using a routine FEM analysis, the prediction of surface settlement is usually not as accurate (e.g., Burland, 1989). Previous studies (Simpson, 1993; Whittle et al., 1993; Stallebrass and Taylor, 1997; Kung, 2003; Kung 2007a) have shown that the accuracy of surface settlement predictions by FEM can be significantly improved if the soil behaviour at small strain levels can be properly modelled. Based on the aspects mentioned above, it is desirable to utilize the finite element method to analyze the excavation-induced ground movements and building responses simultaneously and further conduct the evaluation of building damage caused by excavation.

In this chapter, the possible factors that may affect ground movements caused by excavation are first discussed. The background and development of numerically predicting excavation-induced wall deflection and ground movement are reviewed and introduced especially on the monitoring of excavation case histories. The development of small strain triaxial testing is also reviewed. Subsequently, a simplified soil model, the Modified Pseudo-Plasticity model, developed by the author and his colleagues is described in details. A series of small-strain triaxial tests conducted on the undisturbed Taipei silty clay are used to examine the performance of the Modified Pseudo-Plasticity model. Finally, two well-documented excavation case histories, one located in soft-to-medium clay and the other located in stiff clay, are analyzed numerically using the Modified Pseudo-Plasticity model, and then the conclusions are drawn.

2. Possible factors affecting excavation-induced ground movements

The complicated excavation system may be affected by a large number of factors such as wall stiffness, wall length, ground conditions, groundwater, excavation geometry, construction sequences, strut stiffness, workmanship and so on. It is essential to investigate the factors that may affect the excavation-induced wall deflection and ground movements when studying the topic: “Finite element analysis of wall deflection and ground movements caused by braced excavations”. As reported in the previous studies (e.g., Mana and Clough, 1981; O’Rourke, 1981; Wong and Broms, 1989; Hashash and Whittle, 1996; Kung et al.,

2007b), the wall deflection and ground movements are affected by many factors, which may be grouped into three major categories (Kung, 2009):

A) Inherent factors

1. Stratigraphy: such as soil strength, soil stiffness, stress history of soil, and groundwater conditions. In general, larger wall deflection could be induced for an excavation in soils with lower strength and stiffness.
2. Site environment: such as adjacent buildings and traffic conditions. High-rise buildings and heavy traffic adjacent to the excavation site may cause extra wall deflection.

B) Design-related factors

1. Properties of retaining system: including wall stiffness, strut stiffness, and wall length. Larger wall deflection may be expected when using low-stiffness wall.
2. Excavation geometry: including width and depth of excavation. Generally, the wall deflection is approximately proportioned to the excavation depth.
3. Strut prestress: the strut prestress is aimed at making good connection between the strut and the wall. However, the prestress might reduce the wall deflection.
4. Ground improvement: such as jet grouting method, deep mixing method, compaction grouting method, electro-osmosis method, and buttresses. The soil strength and stiffness could be strengthened by ground improvement, which may reduce wall deflection.

C) Construction-related factors

1. Construction methods: such as the top-down method and bottom-up method.
2. Over-excavation: Over-excavation prior to installation of strut may cause larger wall deflection.
3. Prior construction: such as the effect of trench excavation prior to the construction of the diaphragm wall.
4. Construction of concrete floor slab: the thermal shrinkage of the concrete floor slab may result in an increase in the wall deflection.
5. Duration of the construction sequence: the duration of the strut installation or the floor construction. For an excavation in clay, longer duration for installing the strut or constructing the floor slab may cause larger wall deflection due to the occurrence of consolidation or creep of clay.
6. Workmanship: poorer workmanship may cause higher wall deflection.

The reasonable predictions of wall deflection and ground movement may be obtained provided most of factors can be adequately considered in the process of finite element analysis of braced excavation.

3. Literature review on simulation of excavation-induced ground movements

3.1 Discrepancy in ground movement between observation and prediction

The finite element method has been extensively used in the deformation analysis of retention system and ground caused by excavation over the past decades. According to past studies, it is generally acknowledged that wall deflection is relatively easier to predict than the ground movement using the finite element method with the conventional soil constitutive model such as the Modified Cam-clay model (e.g., Atkinson, 1993). As such, with the conventional soil constitutive model, the FEM simulation of the ground movement is often not as accurate as that of the wall deflection. A significant discrepancy in the ground surface settlement between the in-situ measurements and numerical simulations has been

observed and reported. Figure 4 displays the comparison of wall deflection and ground surface settlement at the final excavation stage between observations and predictions. In this figure, the Taipei National Enterprise Center case was analyzed using various soil models, including the hyperbolic model, the Mohr-Coulomb model, and the Modified Cam-clay model. As shown in Fig. 4, the prediction of settlement distribution is not satisfactory, while the predicted wall deflection is considered relatively reasonable. Specifically, the concave distribution of settlement at distances from 0 to 25m predicted using each of the three soil models is signigicantly less than the observed. The difference in the value and location of maximum settlement between observation and prediction is evident. For the zone far away from the wall (the distance larger than 25m), the predicted settlement is greater than the observed. It should be noted that the wall deflection at various construction stages can be accurately predicted using the three soil models although only the wall deflection simulated at the final stage is shown herein.

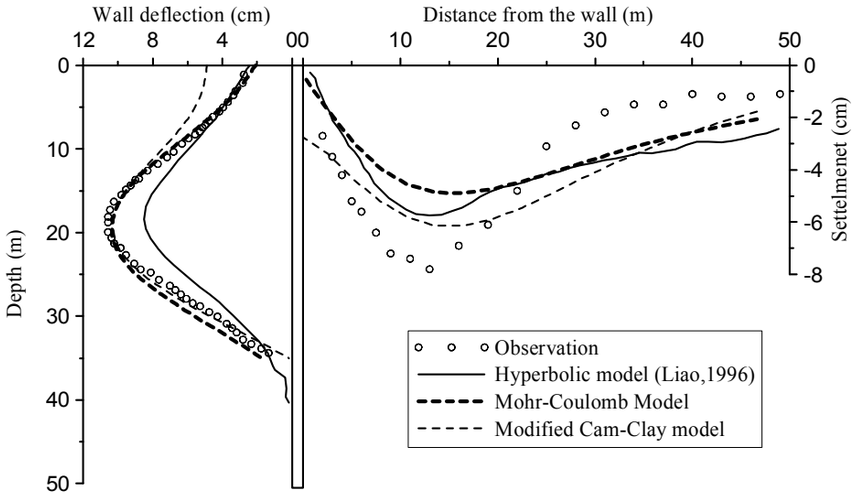

Fig. 4. Performance of various soil models on the simulation of wall deflection and ground surface settlement on the Taipei National Enterprise Center case

The reader may think why the accuracy of predicting the settlement distribution is that important. Essentially, the inaccurate predictions of ground surface settlement by the finite element methon could cause the result that the prevention of building damage near the excavation can not be effectively reached. Figure 5 schematically illustrates the effect of discrepancy in the settlement distribution on the evaluation of damage potential of buildings between actual observations and finite element predictions. For example, if a building is assumed to have no rigidity, finite element predictions tend to underestimate the angular distortion, β, of the building (see Fig. 5) and thus underestimate the damage level of building caused by the excavation-induced settlement.

$$\beta_{prediction} = \delta_{ab} / L \ \square \ \delta_{a'b'} / L = \beta_{observation} \tag{1}$$

where δ represents the differential settlement between adjacent footings and L represents the distance between adjacent footings.

As shown in Fig. 5, use of the surface settlement distribution analyzed by finite element method could lead to improper building protection, which might cause damage to adjacent buildings although the prediction of wall deflection is satisfactory. It would be desirable to further study how to improve the accuracy of numerically predicting the ground surface settlement.

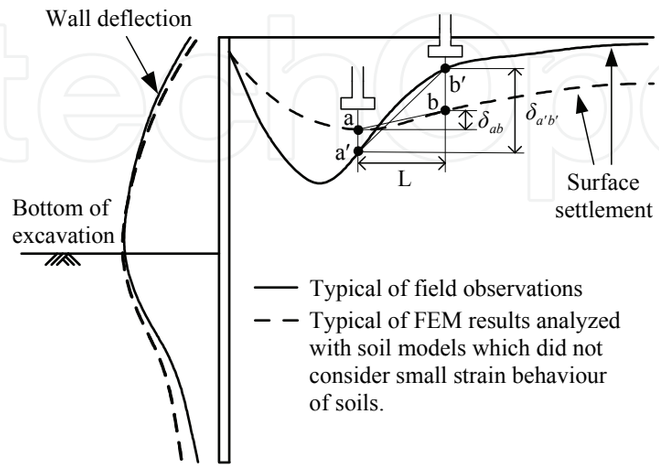

Fig. 5. The inaccurate evaluation of differential settlement of building based on finite element predictions (Kung et al., 2009)

In this section, the in-situ ground observations are utilized to explore the possible factors causing the inaccrute prediction of settlement distribution. Figure 6 shows the excavation-induced shear strain of ground behind the retaining wall observed in the Taipei National Enterprise Center excavation case. The induced shear strain of ground increases with increase of excavation depth. The maximum shear strain of soils at the final excavation depth of 19.7 m is approximately equal to 0.6%. The shear strain of ground far away from the wall is generally less than 0.1%. The stress-strain behaviour of soils at strains less than 0.6 % (or conservatively 1%) for a routine excavation have a dominate effect on the excavation-induced deformation. That is, the capability of the soil model in describing the stress-strain-strength characteristics of soil at small strain levels must be considered when the soil-structure interaction problem is analyzed. Otherwise, the accuracy of predicting excavation-induced ground movements would be significantly reduced.

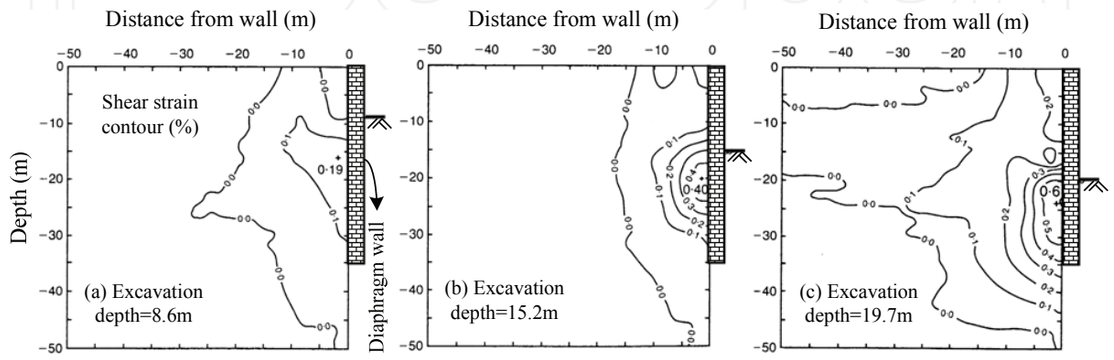

Fig. 6. Excavation-induced shear strain of ground observed in the TNEC case

3.2 Small-strain triaxial testing

The Bishop and Wesley triaxial cell is extensively used in the conventional triaxial test to measure the stress-strain-strength characteristics of soil. The triaxial test is a good method to investigate the soil behaviour, but some studies indicated that results of conventional triaxial tests are reliable only when the measurements of strain are approximately larger than 0.1% (e.g., Atkinson, 1993). Figure 7 displays the typical variation of soil stiffness with the strain from 10^{-4}% to larger than 10%. The degradation of soil stiffness especially at the small stain level is significant. As such, it is believed that the capability of soil model in describing the stress-strain-strength characteristics of soil at a wide range of strain (e.g., 10^{-5} to 10^{-2}) would significantly affect the accuracy in the prediction of excavation-induced ground movements. In other words, the capability of a test in measuring the stress-strain-strength characteristics of soil at a wide range of strain plays a crucial role in the prediction of excavation-induced ground movements. Jardine et al. (1984) indicated that the method of measuring soil deformation in the conventional triaxial test using an LVDT installed outside the triaxial cell was inadequate. Also, many studies (e.g., Burland, 1989; Simpson, 1993; Kung 2003) indicated that the stiffness of soil measured in the conventional triaxial test would be significantly smaller than that measured by in-situ tests or triaxial tests equipped with transducers that can measure very small deformation of soil. Thus, a method to directly measure small deformation of soil locally on the sample was proposed. To date, several kinds of small-strain instruments have been developed (e.g., Clayton and Khatrush, 1986; Goto et al., 1991).

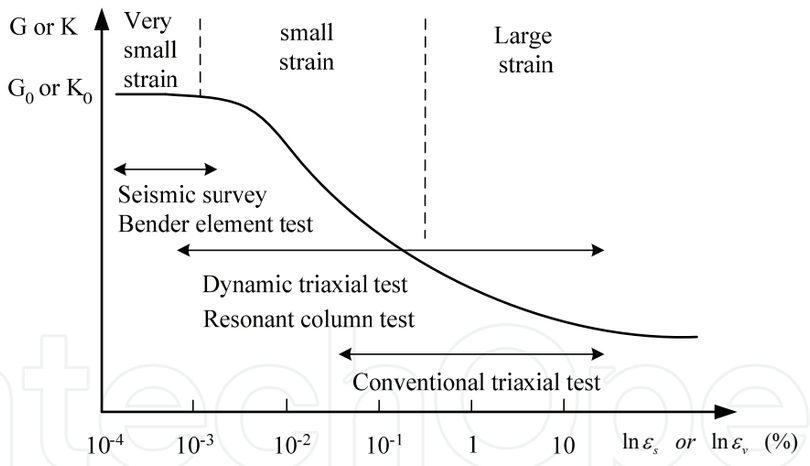

Fig. 7. Variation of soil stiffness with a wide range of strain

Over the past decades, few advanced instruments/transducers were developed for measuring the characteristics of soil at small strain levels (see Fig. 8 and Fig. 9). Figure 8 shows the appearance of bender element and the installation in the top cap and the base pedestal. The bender element composed of two piezoelectric-ceramic chips combined together can be used to measure the shear wave velocity through the sample during the consolidation and shearing stages of triaxial tests. When conducting a bender element test, a function generator is generally used to provide the excitation voltage to one of the bender elements (called the transmitter). The excitation voltage would cause the element to vibrate

and bend, so that a shear pulse is sent through the sample and received by another bender element, i.e. the receiver.

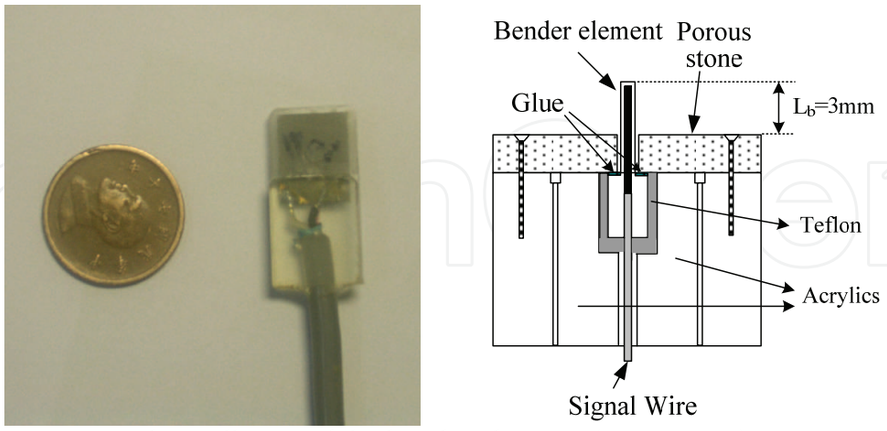

Fig. 8. Appearance and installation of the bender element (Kung, 2007)

Figure 9 exhibits four advanced small strain transducers, including (a) Eletrolevel gauge (Jardine, et al., 1984), (b) Hall effect transducer (Clayton and Khatrush, 1986), (c) Local displacement transducer (Goto, et al., 1991), and (d) Proximity transducer. In addition, the small, light linear variable differential transformer (LVDT) is also available and its installation method is similar to the proximity transducer (Fig. 9d). It should be noted that the principle of measuring the local deformation on a sample with each of the four instruments is not the same. The reader can be referred to references for additional information. It should be noted that some errors may be induced as measuring the stress-strain behavior of soils at small strain using the conventional triaxial apparatus (see Fig. 10). The main errors include manmade errors during preparation of a sample, low precision of instruments, inaccurate measurement methods, and improper arrangement of the conventional triaxial apparatus. Specifically, six kinds of errors may be induced, including (1) rotation of the top cap (2) measurement of loading (3) measurement of deformation (4) environmental temperature (5) disturbance during the preparation of a sample (6) tilting and bedding errors of a sample. Errors No. (1) and (6) are schematically shown in Fig. 11. To date, we can easily purchase the small strain instruments such as the hall effect transducer, the proximity transducer, or the small LVDT, and install them in the existing triaxial apparatus to locally measure the deformation of soils at small strain levels during the triaxial tests. However, it would make a futile effort provided we only substitute a small strain transducer for the original LVDT in a conventional triaxial testing system due to other errors may not be eliminated and the actual behaviour of soil may not be accurately measured (see Fig. 10).

Simply speaking, the force and deformation of a sample should be directly measured on or close to the sample. Use of the local strain transducer and the submerible load cell is a necessity. Obviously, the triaxial cell should be modified to avoid the rotation. Also, the temperature of water during the triaxial test must be measured for calibrating the recorded data. The procedure of preparation and installation of a sample required additional care to prevent the errors (5) and (6). Figure 12 shows an example of the small-strain triaxial testing system, which was developed by the author (Kung 2007).

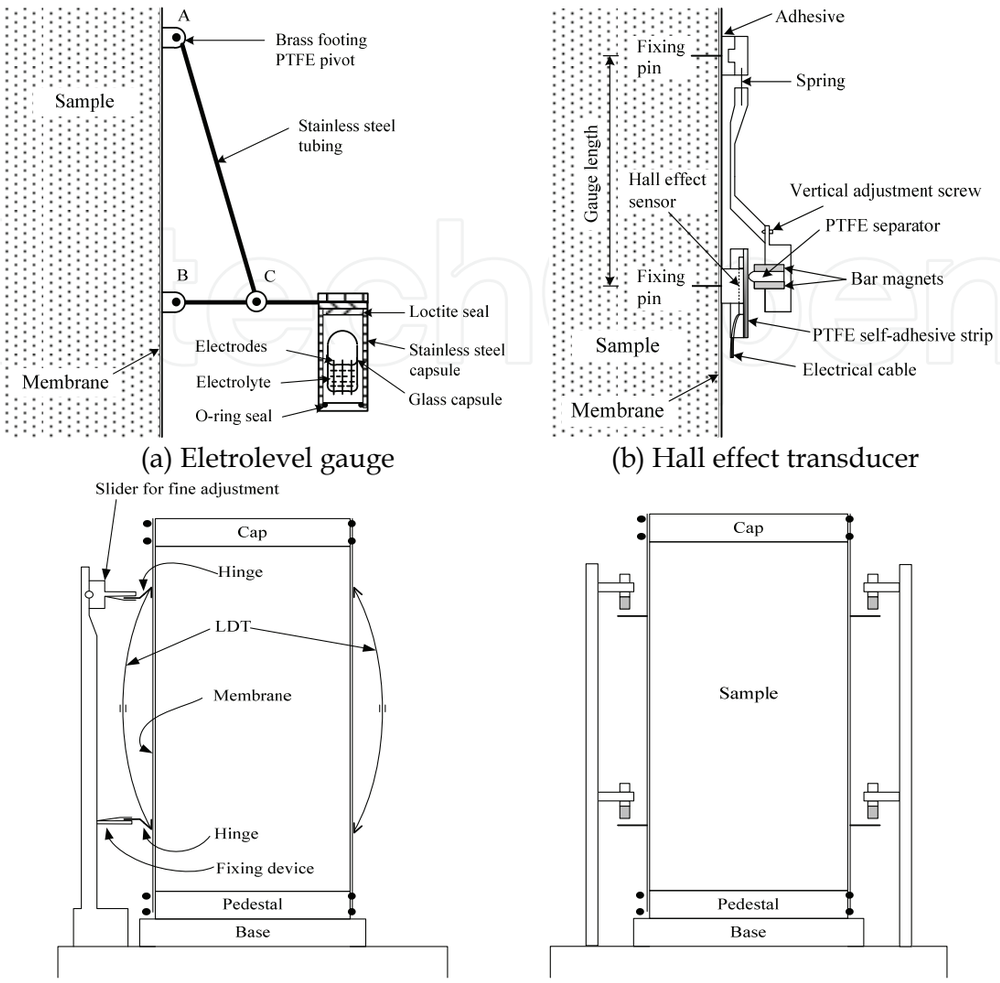

(a) Eletrolevel gauge (b) Hall effect transducer

(c) Local displacement transducer (d) Proximity transducer

Fig. 9. The installation of various small strain transducers on the sample (Kung, 2007)

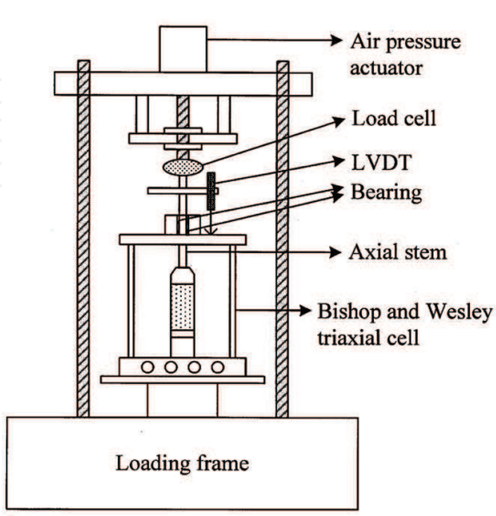

Fig. 10. Layout of the conventional triaxial apparatus (Kung, 2007)

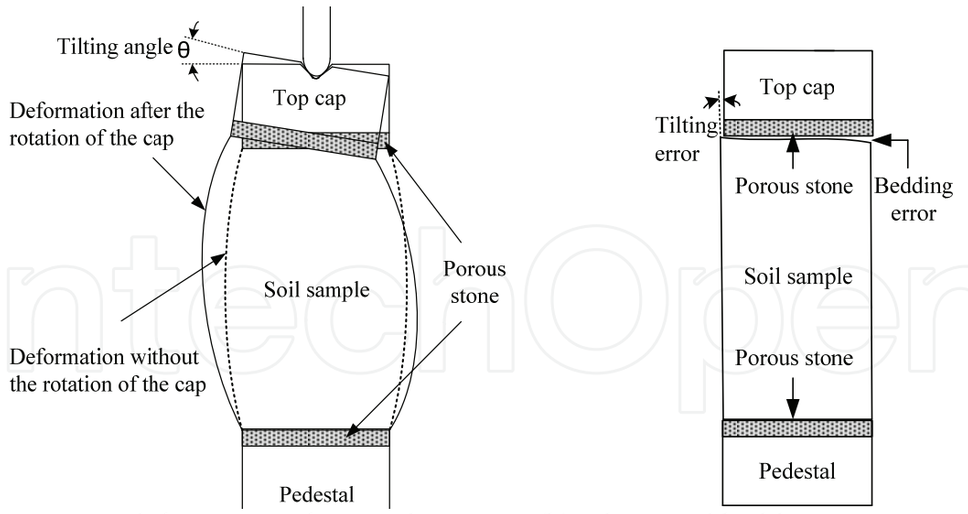

(a) The uneven deformation of a sample due to rotation of the top cap

(b) Tilting and bedding errors caused by set-up of a sample

Fig. 11. Various sources of errors that may be induced by the conventional triaxial apparatus

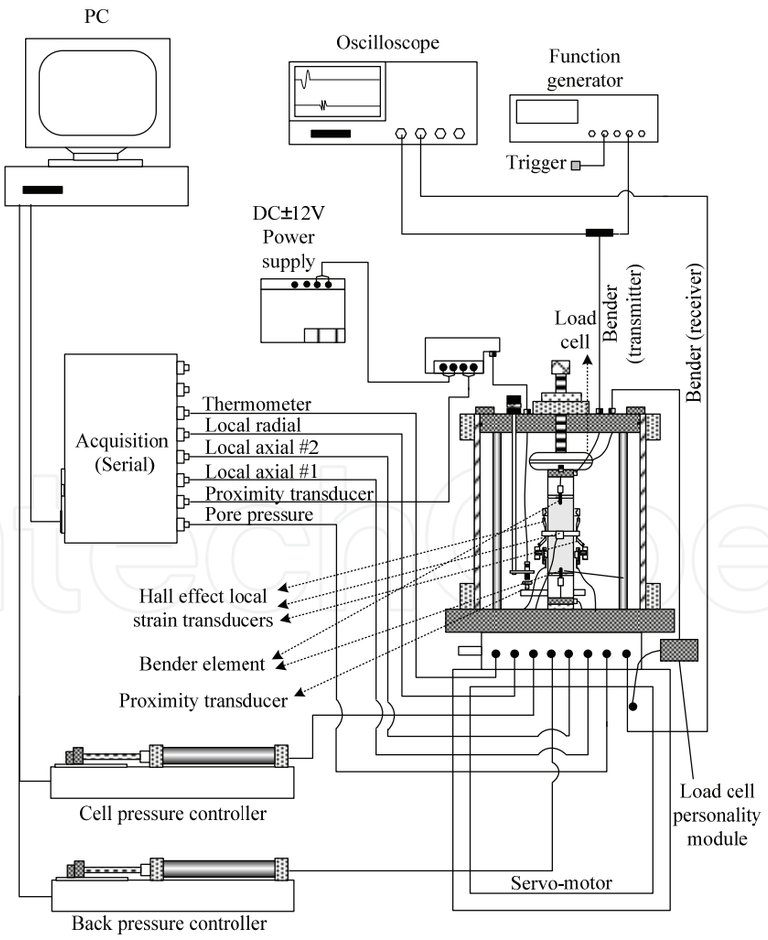

Fig. 12. Layout of the developed small-strain triaxial testing system (Kung, 2007)

4. Development of Modified Pseudo-Plasticity soil model

In recent years, several soil models have been improved to be capable of describing the stress-strain-strength characteristics of soil at small strain levels based primarily on the results of small strain triaxial tests. For instance, Stallebrass and Taylor (1997) incorporated the small strain nonlinear behaviour of soil within the initial yielding surface into the Modified Cam-clay model. The finite element solutions estimated by using this model can improve the discrepancy in the surface settlement between observation and prediction. Although the accuracy of excavation-induced ground movement predictions may be improved by employing a small-strain constitutive model, it could be difficult for engineers to employ such complicated constitutive models in a routine analysis of braced excavation. A simple soil model capable of capturing the small-strain behaviors of soils would be of great interest to practitioners. In this section, a simplified small strain soil model, called the Modified Pseudo-Plasticity model, developed by the author and his colleague are introduced herein and examined.

4.1 Modified pseudo plasticity model

For the Modified Pseudo-Plasticity model, the stress-strain relationship is expressed as follows:

$$\frac{\sigma_1-\sigma_3}{s_{u\beta}}=\frac{\varepsilon}{\frac{s_{u\beta}}{E_i}+\frac{R_f\varepsilon}{2}} \tag{2}$$

where E_i is the initial Young's modulus; $s_{u\beta}$ is the undrained shear strength in the direction of the principal stress axis with an angle of β under the plane-strain condition; R_f is the failure ratio ($=(\sigma_1-\sigma_3)_f/(\sigma_1-\sigma_3)_{ult}$), where $(\sigma_1-\sigma_3)_f$ is the deviator stress at failure and $(\sigma_1-\sigma_3)_{ult}$ is the ultimate deviator stress. The term $s_{u\beta}$ is determined by (see Fig. 13):

$$s_{u\beta}=\left(\sqrt{R^2-(q_c\sin 2\beta)^2}+q_c\cos 2\beta\right)s_{uc} \tag{3}$$

where $q_c=(1-K_s)/2$ and $R=\left[(3K_s+1)(K_s+3)/12\right]^{1/2}$, in which K_s is the ratio of undrained shear strength ($K_s=s_{ue}/s_{uc}$); s_{uc} and s_{ue} are the undrained shear strengths in the triaxial compression and extension tests, respectively; β represents the angle between the direction of the maximum principal stress axis and the vertical direction.
In an incremental analysis, the tangential Young's modulus E_t can be expressed as:

$$E_t=E_{ur}(1-R_fSL)^2 \tag{4}$$

where E_{ur} is the unloading-reloading stiffness; SL is the stress level.

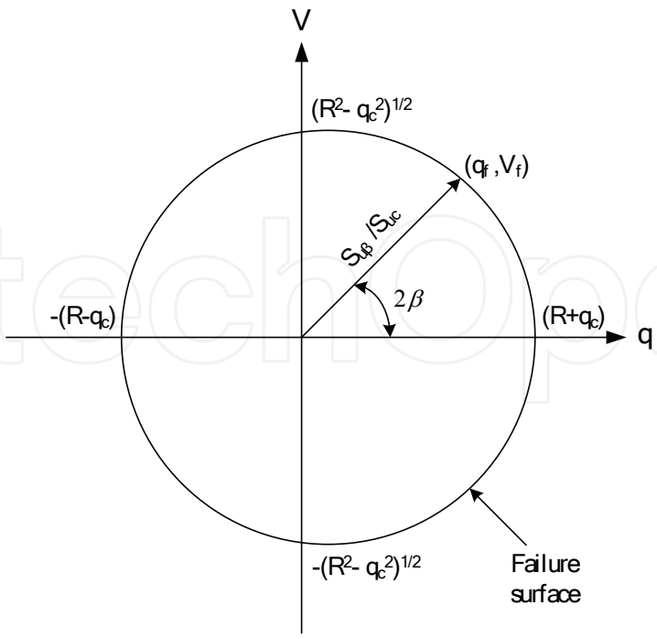

Fig. 13. Undrained shear strength in different directions of the maximum principal stress axis

In the Modified Pseudo-Plasticity model, E_{ur} can be determined by:

$$E_{ur} = E_i \qquad \text{for} \quad \varepsilon \le 10^{-5}\text{, and}$$

$$E_{ur} = E_i[1 - \frac{\varepsilon - 0.00001}{a + b(\varepsilon - 0.00001)}] \qquad \text{for} \quad \varepsilon > 10^{-5} \tag{5}$$

where ε is the axial strain; the coefficients a and b are parameters that control the degradation of stiffness.

The stress level criterion by Prevost (1979), in which the yield surface (S) and the failure surface (F) expressed as Equations 6 and 7 are used to differentiate the states of primary loading and unloading/reloading condition of soil (see Fig. 14), is incorporated into the Modified Pseudo-Plasticity model.

$$F = \frac{\left(\frac{q - q_o(1-SL)}{SL} - q_c\right)^2 + \left(\frac{V}{SL}\right)^2}{R^2} - \Lambda^2 = 0 \tag{6}$$

$$S = \frac{[q - q_c SL - q_o(1-SL)]^2 + V^2}{R^2} - \lambda^2 = 0 \tag{7}$$

where Λ and λ are the parameters defining the magnitude of the failure function and yield surface; q_0 is the normalized initial deviator stress. The stress level (SL) used in Equation 4 can thus be defined as (see Fig. 14):

$$SL = \frac{V}{V_f} = \frac{\left(\frac{\left[q - q_c SL - q_o (1 - SL) \right]^2 + V^2}{R^2} \right)^{\frac{1}{2}}}{\Lambda} \tag{8}$$

In summary, Equations 2 through 8 collectively form the Modified Pseudo-Plasticity model that can describe undrained behavior of clays at various strain levels including small strain. A total of six soil parameters, E_i / s_{uc} , s_{uc} / σ'_v , R_f , K_s , a , and b , are required to define the Modified Pseudo-Plasticity model. In addition, the Poisson's ratio is also required in the finite element analysis. The parameter E_i / s_{uc} can be determined from the small-strain compression triaxial tests at a strain approximately equal to or smaller than 10^{-5}. The parameters s_{uc} / σ'_v and R_f can be determined from the same triaxial compression tests. The parameter K_s can be determined with additional triaxial extension tests. The parameters a and b can be obtained from the multiple unloading/reloading triaxial tests conducted with strains from 10^{-5} to 10^{-2}.

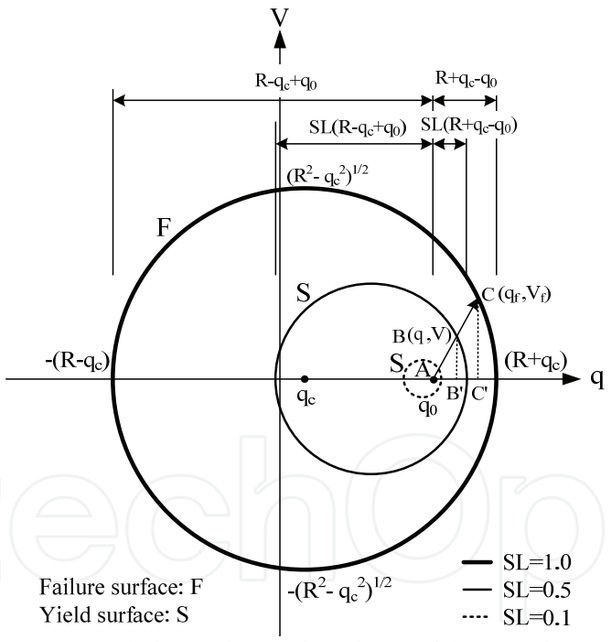

Fig. 14. Undrained shear strength in various directions of the maximum principal stress axis

4.3 Performance of Modified Pseudo-Plasticity model

The performance of the Modified Pseudo-Plasticity model on describing the stress-strain characteristics of clay is evaluated in this section. A number of the undisturbed soil samples were taken from the TNEC case (sites 1 and 2) located in Taipei to conduct the small strain triaxial tests for validating the Modified Pseudo-Plasticity model. Specifically, a total of five K_0-consolidation undrained shearing test (CK_0AC test) as well as two multiple

unloading/reloading shearing tests were conducted. The Modified Pseudo-Plasticity model is then used to simulate the results of the CK_0AC tests and multiple unloading/reloading shearing tests. The samples used in these tests are classified as low plasticity, soft-to-medium silty clay and the basic properties obtained by the test are shown in Table 1. The liquid limit for the samples ranges from 33 to 40, and the plasticity index from 11 to 18. The water contents are in the range of 33%-35%.

Site	Soil types	γ_t	ω (%)	LL (%)	PI (%)
Site 1	CL	18.93	33-35	33-37	12-17
Site 2	CL	18.52	31-33	34-40	11-18

Table 1. Basic properties of soil tested

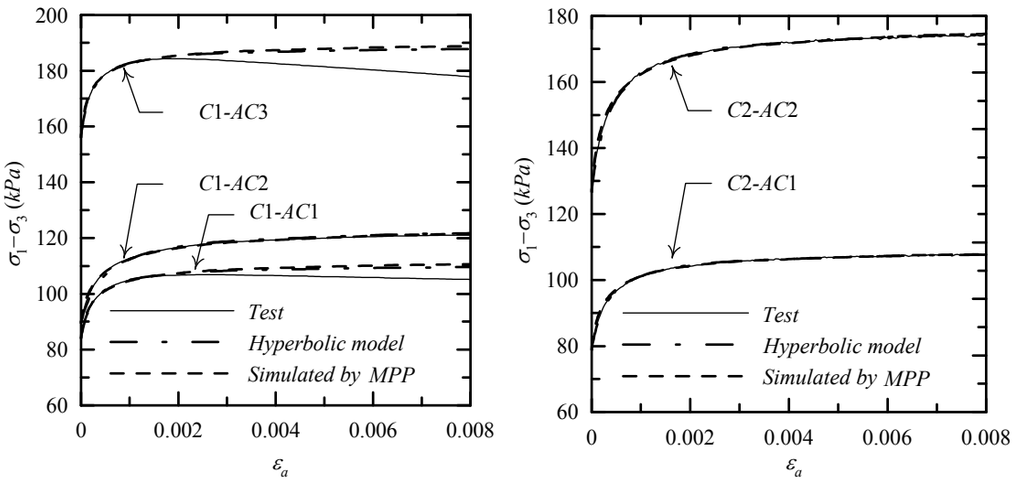

(a) Site 1 (b) Site 2

Fig. 15. Comparison of stress-strain curves between test results and simulations

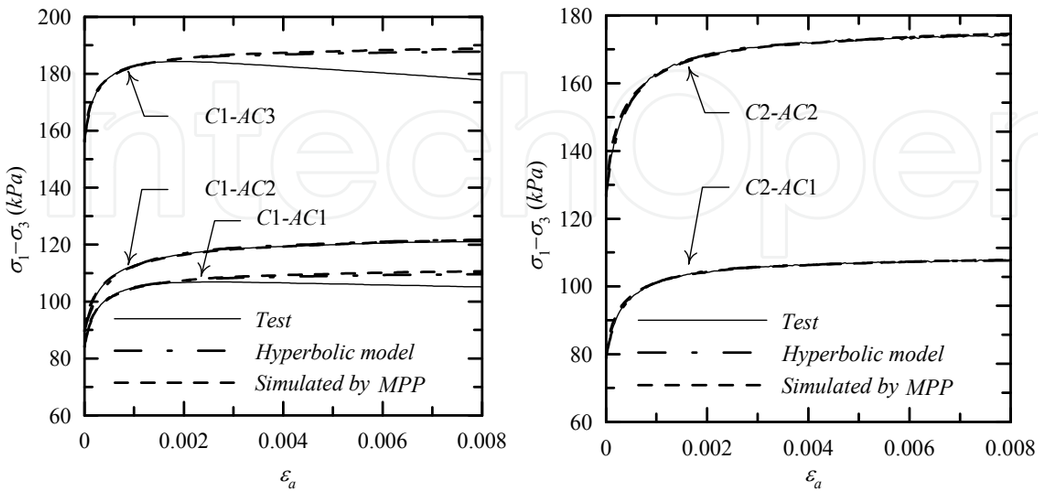

(a) Site 1 (b) Site 2

Fig. 16. Comparison of stiffness-strain relationship between test results and simulations

Figure 15 shows the comparison of stress-strain curves between test results and simulations by the Modified Pseudo-Plasticity model and the hyperbolic model. In general, the stress-strain curves at strains ranging from 0 to 0.008 can be reasonably simulated by the hyperbolic model and the Modified Pseudo-Plasticity model. It can be observed that the softening behaviour of soil (e.g., C1-AC1, C1-AC3) measured at strain larger than 0.002 cannot be appropriately simulated due to the fact that both the hyperbolic model and the Modified Pseudo-Plasticity model are only valid for describing the hardening behaviour of soil. The stiffness-strain relationship of each of five CK_0AC tests is compared and illustrated in Fig. 16. The initial normalized secant stiffness (E_{sec}/s_u) of clay measured by the small strain triaxial tests falls into the range of 2000 to 2200. The values of E_{sec}/s_u obtained by the hyperbolic model are significantly lower than the measured, while the estimation of E_{sec}/s_u by the Modified Pseudo-Plasticity model is satisfactorily consistent with the measured. Overall, the tendency of stiffness degradation of clay can be accurately represented by the Modified Pseudo-Plasticity model.

Finally, Fig. 17 compares the degradation of unloading/reloading modulus (E_e) between test results and simulations. Test results display that the undrained unloading/reloading modulus (E_e) of the Taipei clay decreases with the increase of the axial strain. The simulations shown in this figure exhibit that the variation of unloading/reloading stiffness of clay can be accurately captured by the Modified Pseudo-Plasticity. Compared with the hyperbolic model and the Pseudo-Plasticity model, the unloading/reloading modulus (E_e) assumed by the two soil models is a constant and would be inadequate to be used to predict the excavation-induced ground movements.

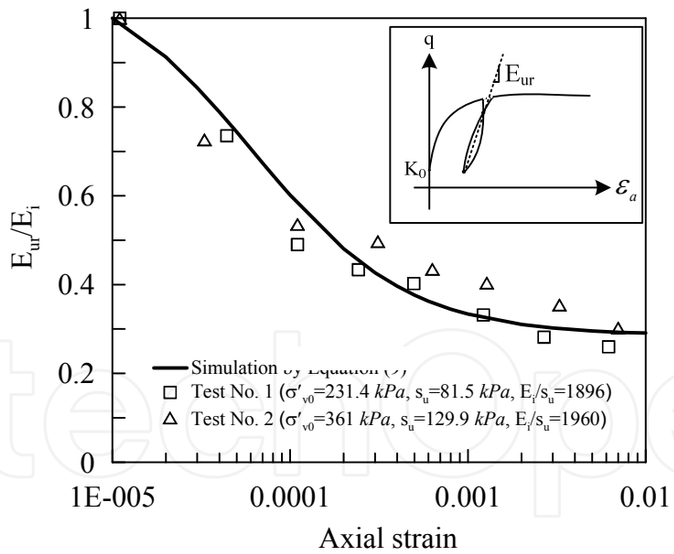

Fig. 17. Comparison of degradation of elastic modulus between test results and simulations

5. Analysis of braced excavation using the Modified Pseudo-Plasticity model

Two well-documented excavation case histories, the Taipei National Enterprise Center case (Ou et al., 1998) and the Post Office Square Garage case (Whittle et al., 1993), are selected to conduct the numerical analyses of excavation for examining the applicability of the Modified Pseudo-Plasticity model.

5.1 Taipei National Enterprise Center excavation case

As shown in Fig. 18, the shape of the Taipei National Enterprise Center case was slightly irregular. The width was 43 m, while the lengths of the southern and northern edges were 106 m and 61 m, respectively. A diaphragm wall, which was 0.9 m thick and 35 m deep, was used as the earth-retaining structure. The foundation of the Taipei National Enterprise Center case was constructed using the Top-down construction method, in which the wall was supported by 150 mm thick solid concrete floor slabs. The maximum excavation depth was 19.7 m. The excavation-induced wall deflection and ground movement were observed through five inclinometers (WI is installed in the wall; SI-1 to SI-4 are installed in the soil), three extensometers and a number of settlement points along the main observation section. Three pairs of inclinometer casings, SI-1, SI-2 and SI-3, and rod-type multipoint extensometers were installed to measure the vertical and horizontal deformation of soil simultaneously.

The Taipei National Enterprise Center case is located in the Taipei Basin, which is generally formed by a thick alluvium formation (the Sungshan Formation) lying above the Chingmei gravel Formation. The thickness of the Sungshan Formation is around 40 to 50 m. Essentially, the Sungshan Formation has six alternating silty sand (SM) and silty clay (CL) layers and mainly consists of low-plasticity and slightly over-consolidated soft to medium clay. Typical soil properties of the Sungshan Formation are shown in Table 2. In this case, the soft to medium clay at depths from 8 m to 33 m has the predominant effect in the excavation-induced deformation behaviour. The Chingmei gravel Formation can be found at the depth of 46 m. The depth of ground water table is around 2 m.

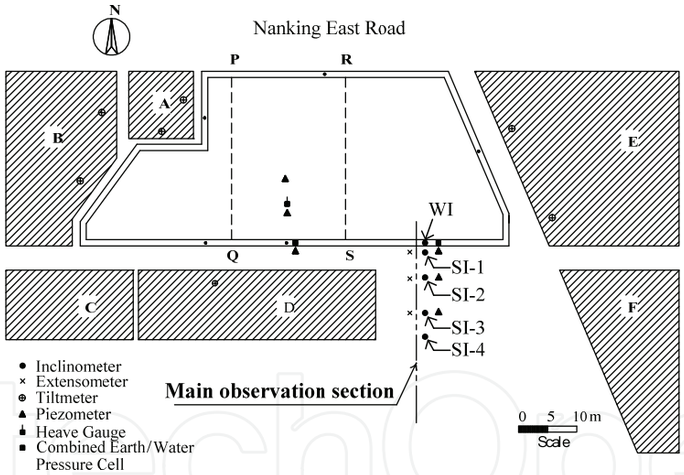

Fig. 18. Plan view of the TNEC case and the instrumentation plan

Formation	Layer	Depth (m)	Soil Type	SPT-N (Blows/ft)	ω_n (%)	LL	PI	ϕ' (°)
Sungshan	VI	0-5.6	CL	3	32	34	23	33
	V	5.6-8.0	SM	11	25	-	-	31
	IV	8.0-33.0	CL	3-10	25-40	29-39	9-19	30
	III	33.0-35.0	SM	20	24	-	-	31
	II	35.0-37.5	CL	14	28	33	21	32
	I	37.5-46.0	SM	30	30	-	-	-
Chingmei		>46.0	GP	>100	-	-	-	-

Table 2. Basic soil properties at the TNEC excavation site.

The considerations and analytical procedures in the analysis of the TNEC case history are described in detail as follows.

(1) Element types

The 8-node rectangular isoparametric quadrilateral element (Q8) was used for soil elements and diaphragm wall elements. The strut during excavation, either steel member or concrete slab, is normally subjected to axial force, and therefore the bar element was used to simulate the behavior of the strut or concrete slab.

(2) Modeling of soil and structure

The diaphragm wall was assumed to behave as a linearly-elastic material, for which both Young's modulus and Poisson's ratio were assumed constant. The clayey soil and sandy soil were assumed to behave as elasto-plastic materials as described by the MPP Model and hyperbolic model, respectively. The undrained analysis for the clayey layers and drained analysis for the sandy layers were employed in the finite element analyses of the TNEC case.

(3) Initial conditions

The effective horizontal stress is equal to the effective vertical stress multiplied by the coefficient of the at-rest lateral earth pressure (K_0) at initial conditions. In the TNEC case, K_0 was determined from the triaxial tests on the undisturbed Taipei clay. The pore water pressure, which was slightly lower than the hydrostatic pressure, was determined from the measurement of the in-situ pore water pressure using piezometers. The total stresses are equal to the sum of effective stress and pore water pressure.

(4) Determination of soil parameters

The MPP model for clay layers and hyperbolic model for sand layers are employed in the analysis. The determination of parameters for hyperbolic model is referred to the original definitions (Duncan and Chang, 1970). As mentioned previously, six soil parameters, E_i / s_u, s_u / σ_v', R_f, a, b and K_s, are required to define the MPP model. The values of E_i / s_u, s_u / σ_v' and K_s were directly determined by the small-strain triaxial tests on the undisturbed Taipei clay sampled from the TNEC case using the local strain instruments and bender element tests simultaneously. Test results showed that E_i / s_u fell in the range from 1600 to 2500 and s_u / σ_v' varied from 0.30 to 0.35. According to Kung (2003), K_s for the Taipei clay is approximately equal to 0.75. For the term R_f, the value of R_f =0.9 is considered adequate to simulate the stress-strain characteristics in the analysis. The results of the multiple unloading/reloading tests can be adequately represented by Equation 5 with $a = 0.0001$ and $b = 1.4$. The values of the six soil parameters used in the analysis are listed in Table 3.

Depth (m)	γ_t (kN/m³)	K_0	E_i / s_u	s_{uc} / σ_v'	R_f	a	b	ν	K_s
0-5.6	18.3	1.0	2100	0.32	0.9	0.0001	1.4	0.499	0.75
8-33	18.9	0.51	2100	0.32	0.9	0.0001	1.4	0.499	0.75
35-37.5	18.2	0.51	2100	0.34	0.9	0.0001	1.4	0.499	0.75

(a) Parameters of clayey layers (MPP model)

Depth (m)	γ_t (kN/m^3)	K_0	c′ (kPa)	ϕ′ (°)	R_f	K= K_{ur}	n	ν
5.6-8	18.9	0.49	0	31	0.9	750	0.5	0.3
33-35	19.6	0.49	0	31	0.9	2500	0.5	0.3
37.5-46	19.6	0.47	0	32	0.9	2500	0.5	0.3

(b) Parameters of sandy layers (Hyperbolic model)

Table 3. Soil parameters used in finite element analyses of the TNEC case

(5) Determination of structural parameters

The nominal Young's modulus of diaphragm wall (E_c) can be calculated by:

$$E_c = 4700\sqrt{f_c'} \tag{9}$$

where f_c' is the compressive strength of concrete (MPa).

For the FEM analysis of braced excavation, the nominal E_c is reduced to account for the effect of underwater construction of the diaphragm wall. In this study, 80% of nominal E_c is taken to conduct the FEM analysis. In the TNEC case, f_c' is equal to 27.44 MPa. The stiffness of struts or floor slabs, k, is determined by:

$$k = EA/LS \tag{10}$$

where E is Young's modulus of steel or concrete; A is the cross-section area; L is the length; S is the horizontal span. The stiffness of struts and floor slabs adopted are shown in Table 4. Figure 19(a) shows the comparison of the wall deflection between field observations and FEM predictions. The cantilever-type wall deflection at first and second stages can be accurately estimated. After the construction of concrete floor slabs, the deep-inward movements of wall deflection were induced at subsequent stages. The calculated maximum wall deflections are very close to the observations at stages 3 to 7, while the locations where the maximum wall deflection occurred can be accurately estimated except stages 6 and 7, where the estimated position is slightly deeper than the observations. The calculated maximum wall deflection is 109 mm, which is practically identical to the measured.

Stage No.	TNEC case			POSG case		
	H_e (m)	H_p (m)	k (kN/m/m)	H_e (m)	H_p (m)	k (kN/m/m)
1	2.8	N/A	N/A	2.8	-	-
2	4.9	2.0	8240	6.1	0.4	482623
3	8.6	3.5 & 0	125568	8.3	3.1	168918
4	11.8	7.1	125568	11.6	6.4	168918
5	15.2	10.3	125568	14.5	9.5	168918
6	17.3	13.7	125568	17.1	12.5	168918
7	19.7	16.5	24035	20.1	15.6	180984
8	-	-	-	23.2	18.6	180984

Note: H_e is the excavation depth; H_p is the depth where the strut is installed; k denotes the stiffness of strut and floor slab

Table 4. Propping arrangements for the excavation case histories and stiffness of struts and floor slab used in FEM analyses

Figure 19(b) shows the comparison of ground surface settlement. The observations reveal that the concave shape of surface settlement was induced mainly at distances of 0 to 25 m away from the wall. The maximum surface settlement after the completion of the final excavation stage (stage 7, excavation depth = 19.7 m) is around 74 mm and the location where the maximum surface settlement occurred is 13 m away from the wall. The results show that the trend of the settlement profile is fairly accurately estimated.

The predicted surface settlement at the range of 0 to 25 m away from the wall compare well to the observations, but the predictions of the surface settlement at the range of 25 to 40 m away from the wall are slightly larger than the observations. Generally, predictions of the maximum surface settlement at each stage are considered satisfactory except that at stages 5, 6, and 7, the maximum surface settlement is slightly underestimated.

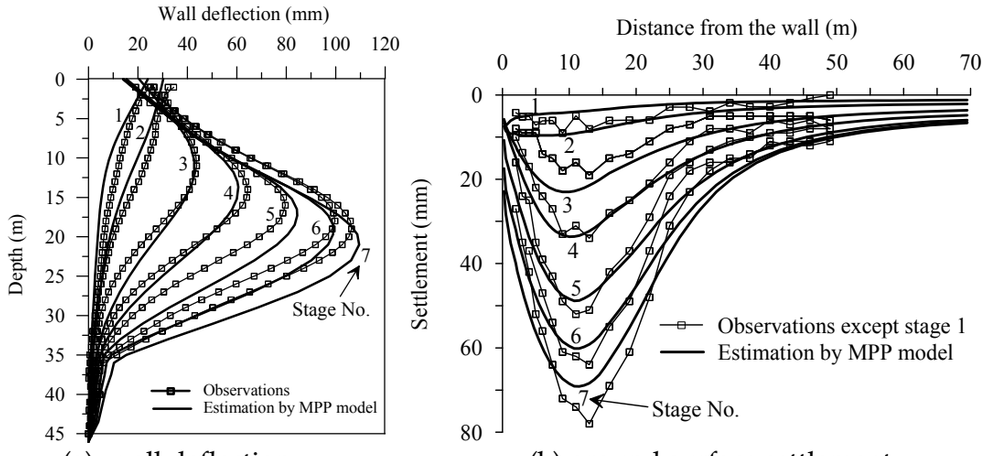

(a) wall deflection (b) ground surface settlement

Fig. 19. Comparison of wall deflection and ground surface settlement

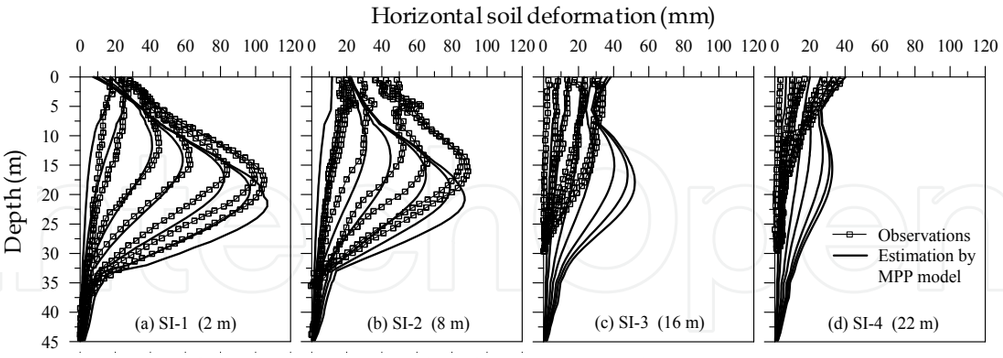

Fig. 20. Comparison of the horizontal soil deformation in the TNEC case

Figure 20 shows the comparison of the horizontal soil deformation. The results show that the computed maximum horizontal soil deformation and profiles along the SI-1 and SI-2 sections are generally close to the observations, although the difference is observed for the location where the maximum horizontal soil deformation occurred at the final two stages. However, the soil deformation along the SI-3 and SI-4 sections are accurately predicted at depths smaller than 10 m and over-predicted at depths larger than 10 m. Moreover,

compared with predictions of the vertical settlement, both the vertical and horizontal soil deformation were overestimated by the MPP model in the distance range of 25 to 40 m.
In view of the difficulty of obtaining satisfactory predictions of all three responses (wall deflection, surface settlement, and horizontal soil deformation) simultaneously with a finite element analysis, the results obtained using the Modified Pseudo-Plasticity soil model are considered satisfactory.

5.2 Post Office Square Garage case

The observations during construction in the Post Office Square Garage (POSG) excavation case history were performed by Whittle et al. (1993). As shown in Fig. 21(a), this case occupies a plan area of 6880 m² (approximately 116×61 m) in the heart of financial district of Boston. Existing buildings up to 40 stories tall are located adjacent to the site. The diaphragm wall (25.6 m deep and 0.9 m thick) extending down into the bedrock was used as the permanent lateral earth pressure support. The POSG case was performed by the Top-down construction method. The maximum excavation depth was 23.2 m. The detailed construction sequences, including the excavation depth and the depth where the floor slab was constructed, are listed in Table 4. .
Figures 21(b) and 21(c) show the plan view of inclinometers and surface settlement points installed around the site, respectively. There are 13 inclinometers cast within the wall and 11 inclinometers located either in front of adjacent buildings or in close proximity to the diaphragm wall. Besides, Whittle et al. (1993) also installed six multiple position borehole extensometers to measure the relative vertical displacement of the clay, till and rock and 5 observation wells and 30 piezometers to measure the ground-water and piezometric level.
Based on an averaged profile of subsurface stratigraphy interpreted from a series of 15 borings conducted at the site, the stratigraphy mostly consists of the fill layer, clay, sand, till and bedrock. The fill layer comprises a heterogeneous mixture of sand, sandy gravel and construction debris. Underlying the fill is a deposit of low plasticity (I_p=20-30%), moderately sensitive (s_t = 3-6) clay containing numerous lenses of sand layers. The results of oedometer tests show that the clay has an in-situ over-consolidation ratio decreasing with depth in the deposit and ranging from OCR = 2-6. The soil deposits overlying the bedrock are classified as glacial till comprising a very heterogeneous mixture of particles, ranging from silt-size to cobbles and boulders. Finally, the bedrock is a moderately to severely weathered argillite deposit containing discontinuous layers of sandstone and quartzite.

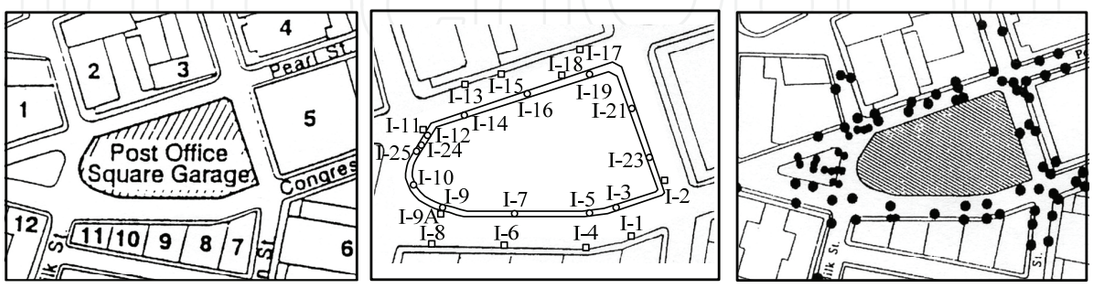

(a) Plan view of POSG case and adjacent buildings (b) Inclinometer location plan (c) Surface settlement point plan

Fig. 21. Plan view of the POSG case and the instrumentation plan (after Whittle et al., 1993)

The values of the six soil parameters used in the analysis of the POSG case are listed in Table 5. According to the results of FEM analyses on the POSG case history using the Modified Pseudo-Plasticity soil model, the results of simulations of the wall deflection, ground surface settlement, and horizontal soil deformation behind the wall are extracted to compare with the observations. Before comparing the analysis results with observations, it is necessary to identify if the two-dimensional FEM analyses conducted under the plane strain condition are comparable to the complicated three-dimensional excavation observations. As shown in Fig. 21(b), a total of 13 inclinometers were installed in the wall to observe the wall deflection during excavation. Considering the arrangement of inclinometers and plane-strain condition, this study carried out the FEM analysis with a cross-section perpendicular to the long side and compared results of analysis with measurements of I-5, I-7 and I-16 because those inclinometers are located at the positions close to the central zone of diaphragm wall. According to the PSR concept proposed by Ou et al. (1996), the locations of I-5, I-7 and I-16 fall into the range of plane strain condition in light of values of PSR very close to 1.0. Therefore, the two-dimensional FEM analysis results of the POSG case would be comparable to the measurements of I-5, I-7 and I-16.

Figure 22 shows the comparison of wall deflection between the estimations by the MPP model and measurements of I-5, I-7 and I-16. At the first stage, the cantilever-type wall deflections can be appropriately simulated and the estimations are very close to the measurements of I-7 but slightly less than those of I-5 and I-16. At the second stage, the estimated wall deflection behaves the deep-inward behavior due to the fact that the high-stiffness concrete floor slab at depth of 0.4 m was constructed prior to the second-stage excavation. However, such cantilever-type wall deflection analyzed doesn't agree with the measurements of I-5, I-7, and I-16. The maximum wall deflection estimated at the second stage is practical equal to that observed by I-5 and I-7, but significantly smaller than that observed by I-16. Also, the depth where the maximum wall deflection occurred at the second stage (≈7m) for the FEM simulations is obviously different from the observations, in which the maximum wall deflection is induced at the ground surface level. This difference in the wall deflection profile between estimations and observations may be caused by effect of long time required to construct the concrete floor slab at ground surface level and its thermal shrinkage. The deep-inward wall deflection was observed at stages 3 to 7. Essentially, the estimated wall deflection profiles, the maximum wall deflection, and the location where the maximum wall deflection occurred generally fall into the range of measurements of I-5, I-7, and I-16. Overall, the estimated wall deflections using the MPP soil model are satisfactory.

Figure 23 shows the comparison of ground surface settlement between estimations and observations. In this figure, all the surface settlement observations recorded around the site were collected to compare with the estimations since the POSG case is located in the heart of financial district of Boston and there is not enough space to measure the profile of ground surface settlement along a specific section perpendicular to the diaphragm wall.

Depth (m)	γ_t (kN/m^3)	K_0	E_i / s_u	s_{uc} / σ'_v	R_f	a	b	ν	K_s
0-2.4	19.2	1.0	2100	0.70	0.9	0.00001	1.2	0.499	0.55
2.4-15.6	19.6	1.0	2100	0.70	0.9	0.00001	1.2	0.499	0.55

(a) For clayey layers

Depth (m)	γ_t (kN/m^3)	K_0	c′ (kPa)	ϕ′ (°)	R_f	K= K_{ur}	n	ν
15.6-17.1	19.6	0.4	0	37	0.9	1500	0.5	0.3
17.1-23.2	20.4	0.5	0	43	0.9	1000	0.5	0.3
23.2-25.6	22.0	1.0	175	32	0.9	3000	0.5	0.3
25.6-45.6	22.0	1.0	300	32	0.9	4000	0.5	0.3

(b) For sandy layers

Table 5. Soil parameters used in FEM analyses of the POSG case

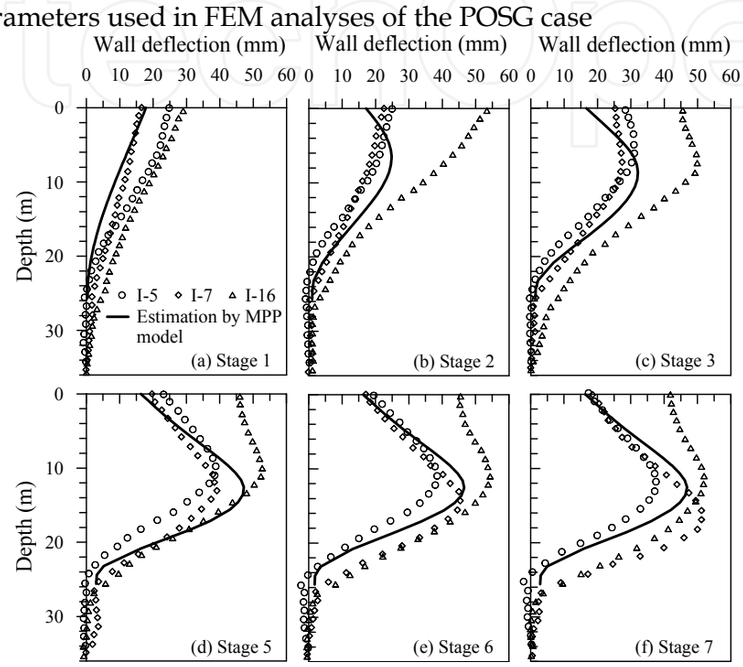

Fig. 22. Comparison of wall deflection (Kung, 2010)

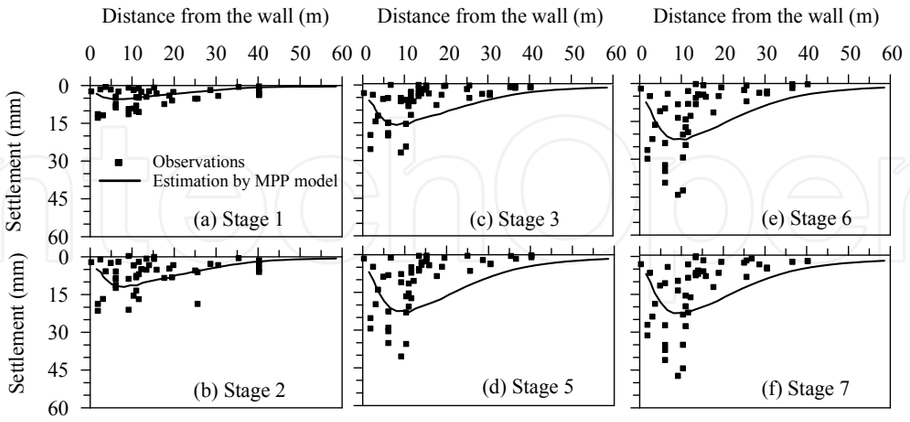

Fig. 23. Comparison of ground surface settlement (Kung, 2010)

Theoretically, the ground surface settlement distrubution obtained by the two-dimensional FEM analysis under the plane strain condition should be an envelope; namely, all surface settlement observations should not exceed the envelope. Past studies indicated that for a practical excavation case, it is common to receive the settlement observations that are larger

than the estimated distribution analyzed by the two-dimensional FEM due to the fact that many factors such as the uncertainty of stratigraphy, variation of construction sequences, and traffic condition are not usually consistent with the design conditions. As shown in Fig. 22, amounts of part of surface settlement observations, especially in the range of 0-10 m behind the wall, are larger than that estimated by the MPP soil model, irrespective of excavation stages. Although the maximum surface settlement was underestimated at each stage, most of surface settlement measurements are smaller than the estimations, while the variation of settlement with the distance from the wall is consistent with the estimated settlement profile.

Figure 24 compares estimated horizontal soil deformations with in-situ data observed from inclinometers located at distance of 4, 9, and 14 m behind the wall. Specifically, the horizontal soil deformation recorded by I-2 and I-18 (4m behind the wall), I-13, I-15, and I-17 (9m behind the wall), and I-1 and I-8 (14m behind the wall) are extracted to compare with the estimations. The locations of those inclinometers can be referred to Fig. 21(b). For the condition of 4 m behind the wall, observations of I-2 and I-18 at stage 1 can be reasonably estimated (solid line). For stages 4 and 7, the estimated horizontal soil deformation would slightly overestimate the observations of I-18 but significantly overestimate those of I-2. The possible reason is due to the fact that I-2 is located at the corner and the deformation would be reduced by the corner effect. It may not be appropriate to directly compare the estimations with the observations of inclinometers, which are not located at the middle area of wall. Accordingly, this study employed PSR concept suggested by Ou et al. (1996) to further compare the horizontal soil deformation.

Briefly, PSR can be defined as the ratio of the maximum deflection in an arbitrary section to that computed under plane strain conditions (the same excavation width). For the scenario of 4 m behind the wall, the value of PSR is determined to be approximately equal to 0.8 and used to modify the FEM estimations. As shown in Fig. 24, the scaling estimations are closer to the observations of I-18 at later stages. The estimation of the maximum horizontal soil deformation at stage 7 is satisfactory. For the condition of 9m behind the wall, the horizontal soil deformation at stage 1 can be accurately estimated, while the maximum horizontal soil deformation at stage 7 can be accurately estimated but the estimated profile is not satisfactory.

For the condition of 14 m behind the wall, the horizontal soil deformation would be significantly overestimated because I-1 and I-8 are located at the zone closer to the corner. The value of PSR for I-1 and I-8 approximately equal to 0.2 is determined based on Ou et al. (1996). Then, the horizontal soil deformation profiles are modified with PSR=0.2 and the results are comparable to the observations. The corner effect on excavation behavior is significant and the additional attention should be paid when comparing the observations with the analysis results, which are obtained using two dimensional finite element analysis.

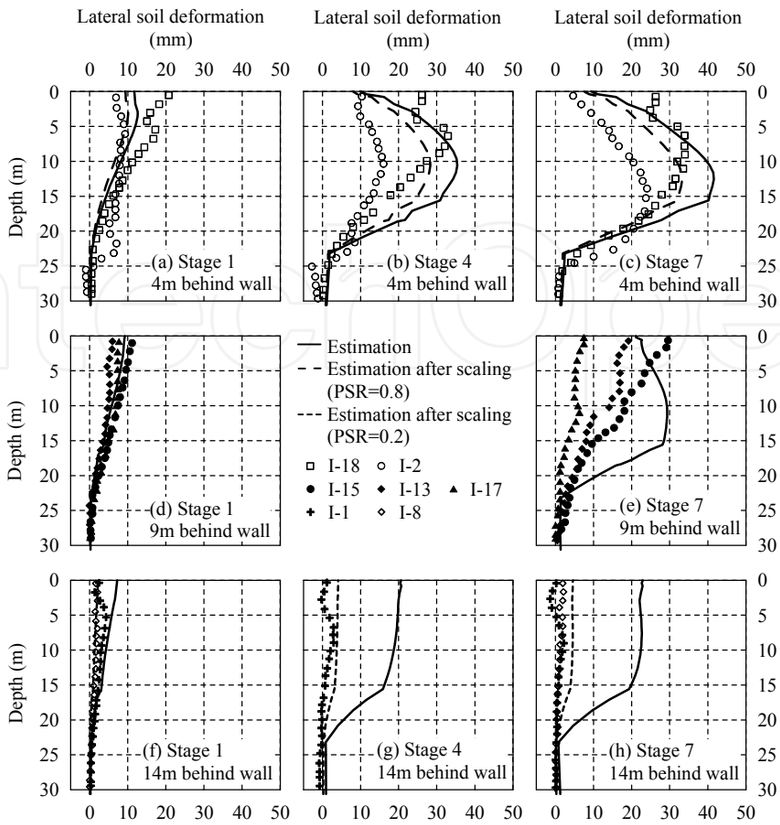

Fig. 24. Comparison of lateral soil deformations (Kung, 2010)

6. Conclusions

To accurately predict excavation-induced ground movements is a complicated but essential task in a routine excavation design for achieving the goal to prevent the damage to buildings adjacent to excavation. Use of numerical methods, such as the finite element method, to predict the ground movements caused by excavation is advantageous due to the stress and strain of the retention system and ground can be provided in the numerical analysis. The analysis results show that the capability of the soil model adopted in describing the stress-strain-strength of characteristics of soils at a wide range of strain, especially at small strain ranging from 10^{-5} to 10^{-2}, plays the crucial role in accurately predicting the excavation-induced ground movements. In addition, the engineer also has to realize the importance of small strain triaxial tests, which can be employed to be a basis for developing the above-mentioned small strain soil models and to measure the soil parameters of small strain soil models for deformation analysis of excavation. Indeed, it is not a simple work to perform such numerical analysis of excavation using small strain soil models but it would significantly benefit the excavation design. The Modified Pseudo-Plasticity model developed is merely one of qualified soil models. The engineer is strongly encouraged to study such numerical analysis of excavation using the small strain soil model and employ in the future design of excavation. Of course, use of small strain soil models to develop new simplified methods for the prediction of excavation-induced ground movements and building responses is desirable.

7. References

Atkinson, J.H. (1993). An Introduction to the Mechanics of Soils and Foundations:/ through critical state soil mechanics, McGraw-Hill, ISBN:007707713X , London.

Burland JB. (1989).Ninth Laurits Bjerrum memorial lecture: small is beautiful-the stiffness of soils at small strain. Canadian Geotechnical Journal, Vol. 26, 499–516, ISSN:1208-6010.

Clayton, C.R.I. & Khatrush, S.A. (1986). A New Device for Measuring Local Axial Strains on Triaxial Specimens. Geotechnique, Vol. 36, 593-597, ISSN: 0016-8505.

Clough, G.W. & O'Rourke, T.D. (1990). Construction-induced movements of in-situ walls. Proceeding of Specialty Conference on Design and Performance of Earth Retaining Structure, pp. 439-470, American Society of Civil Engineers, ISBN: 0872627616, Cornell University, June 1990, Ithaca, New York.

Duncan, J.M. & Chang, C.Y. (1970). Nonlinear Analysis of Stress and Strain in Soils. Journal of the Soil Mechanics and Foundations Division, Vol. 96, No. 5, 637-659, ISSN: 1090-0241.

Finno, R.J. & Harahap, I.S. (1991). Finite element analysis of HDR-4 excavation. Journal of Geotechnical and Geoenvironmental Engineering, Vol. 117, No. 10, 1590–1609, ISSN: 1090-0241.

Goto, S.; Tatsuoka, F.; Shibuya, S.; Kim, Y.S. & Sato, T. (1991). A Simple Gauge for Local Small Strain Measurements in the Laboratory. Soil and Foundations, Vol. 31, No. 1, 169-180, ISSN: 0038-0806.

Hashash, Y.M.A. & Whittle, A.J. (1996). Ground movement prediction for deep excavations in soft clay. Journal of the Geotechnical Engineering, Vol. 122, No. 6, 474–486, ISSN: 1090-0241.

Hsieh, P.G. & Ou, C. Y. (1998). Shape of ground surface settlement profiles caused by excavation. Canadian Geotechnical Journal, Vol. 35, No. 6, 1004–1017, ISSN:1208-6010.

Jardine, R.J.; Symes, M.J. & Burland, J.B. (1984). The measurement of Soil Stiffness in the Triaxial Apparatus. Geotechnique, Vol. 34, No. 3, 323-340, ISSN: 0016-8505.

Kung, G.T.C. (2003). Surface settlement induced by excavation with consideration of small strain behavior of Taipei silty clay. PhD Dissertation, Department of Construction Engineering, National Taiwan University of Science and Technology, Taipei, Taiwan.

Kung, G.T.C. (2009). "Comparison of excavation-induced wall deflection using top-down and bottom-up construction methods in Taipei silty clay." Computers and Geotechnics, Vol. 36, No. 3, 373-385, ISSN: 0266-352X.

Kung, G.T.C. (2010). Modeling small-strain nonlinearity of soils for numerical simulation of braced excavation in stiff clay. Advances in Computer Science and Engineering, Vol. 4, No. 1, 1-21, ISSN: 0973-6999.

Kung, G.T.C.; Hsiao, E.C.L. & Juang, C.H. (2007a). Evaluation of a simplified small strain soil model for estimation of excavation-induced movements. Canadian Geotechnical Journal, Vol. 44, 726–736, ISSN:1208-6010.

Kung, G.T.C.; Juang, C.H.; Hsiao, E.C.L. & Hashash, Y.M.A. (2007b). Simplified model for wall deflection and ground surface settlement caused by braced excavation in clays. Geotechnical and Geoenvironmental Engineering, Vol. 133, No. 6, 731-747, ISSN: 1090-0241.

Kung, G.T.C.; Ou, C.Y. & Juang, C.H. (2009). Modeling small-strain behaviour of Taipei clays for finite element analysis of braced excavations. Computers and Geotechnics, Vol. 36, No. 1-2, 304-319, ISSN: 0266-352X.

Liao, J.T. (1996). Performances of a Top Down Deep Excavation, Ph.D. Dissertation, Department of Construction Engineering, National Taiwan University of Science and Technology, Taipei, Taiwan.

Mana, A.I. & Clough, G.W. (1981). Prediction of movements for braced cut in clay. Journal of the Geotechnical Engineering, Vol. 107, No. GT8, 759-777, ISSN: 1090-0241.

Ng, C.W.W. & Yan, W.M. (2000). A true three-dimensional numerical analysis of diaphragm walling. Geotechnique, Vol. 49, No. 6, 825–834, ISSN: 0016-8505.

O'Rourke, T.D. (1981). Ground movements caused by braced excavations. Journal of the Geotechnical Engineering, Vol. 107, No. 6, 1159-1177, ISSN: 1090-0241.

Ou, C.Y., Chiou, D.C. & Wu, T.S. (1996). Three-dimensional finite element analysis of deep excavations, Journal of the Geotechnical Engineering, Vol. 122, No. 5, 337-345, ISSN: 1090-0241.

Ou, C.Y.; Liao, J.T. & Lin, H.D. (1998). Performance of Diaphragm Wall Constructed Using Top-down Method. Journal of Geotechnical and Geoenvironmental Engineering, Vol. 124, No. 9, 798-808, ISSN: 1090-0241.

Prevost, J.H. (1979). Undrained shear tests on clay. Journal of the Geotechnical Engineering, Vol. 105, No. 1, pp. 49-64, ISSN: 1090-0241.

Simpson, B. (1993). Development and application of a new soil model for prediction of ground movements, Proceedings of the Wroth Memorial Symposium, pp. 628-643, ISBN:0727719165, St Catherine's College, Oxford, July 1992, Oxford, London.

Stallebrass, S.E. & Taylor, R.N. (1997). The development and evaluation of a constitutive model for the prediction of ground movements in overconsolidation clay. Geotechnique, Vol. 47, No. 2, 235–253, ISSN: 0016-8505.

Whittle, A.J.; Hashash, Y.M.A. & Whitman, R.V. (1993). Analysis of deep excavation in Boston. Journal of the Geotechnical Engineering, Vol. 119, No. 1, 69–90, ISSN: 1090-0241.

Wong, K.S. & Broms, B.B. (1989). Lateral wall deflections of braced excavation in clay. Journal of the Geotechnical Engineering, Vol. 115, No. 6, 853-870, ISSN: 1090-0241.

Finite Element Analysis

Edited by David Moratal

ISBN 978-953-307-123-7

Hard cover, 688 pages

Publisher Sciyo

Published online 17, August, 2010

Published in print edition August, 2010

Finite element analysis is an engineering method for the numerical analysis of complex structures. This book provides a bird's eye view on this very broad matter through 27 original and innovative research studies exhibiting various investigation directions. Through its chapters the reader will have access to works related to Biomedical Engineering, Materials Engineering, Process Analysis and Civil Engineering. The text is addressed not only to researchers, but also to professional engineers, engineering lecturers and students seeking to gain a better understanding of where Finite Element Analysis stands today.

How to reference

In order to correctly reference this scholarly work, feel free to copy and paste the following:

Gordon Tung-Chin Kung (2010). Finite Element Analysis of Wall Deflection And Ground Movements Caused by Braced Excavations, Finite Element Analysis, David Moratal (Ed.), ISBN: 978-953-307-123-7, InTech, Available from: http://www.intechopen.com/books/finite-element-analysis/finite-element-analysis-of-wall-deflection-and-ground-movements-caused-by-braced-excavations

INTECH
open science | open minds

InTech Europe
University Campus STeP Ri
Slavka Krautzeka 83/A
51000 Rijeka, Croatia
Phone: +385 (51) 770 447
Fax: +385 (51) 686 166
www.intechopen.com

InTech China
Unit 405, Office Block, Hotel Equatorial Shanghai
No.65, Yan An Road (West), Shanghai, 200040, China
中国上海市延安西路65号上海国际贵都大饭店办公楼405单元
Phone: +86-21-62489820
Fax: +86-21-62489821

© 2010 The Author(s). Licensee IntechOpen. This chapter is distributed under the terms of the Creative Commons Attribution-NonCommercial-ShareAlike-3.0 License, which permits use, distribution and reproduction for non-commercial purposes, provided the original is properly cited and derivative works building on this content are distributed under the same license.

IntechOpen

IntechOpen